FLUORESCENT VISUALIZATION FOR TURBOMACHINE RESEARCH

BY

A. H. EPSTEIN

GT&PDL REPORT No. 142 MARCH 1978

GAS TURBINE LABORATORY
MASSACHUSETTS INSTITUTE OF TECHNOLOGY
CAMBRIDGE, MASSACHUSETTS

FLUORESCENT VISUALIZATION FOR TURBOMACHINE RESEARCH

BY

A. H. EPSTEIN

GT&PDL REPORT NO. 142 MARCH 1978

THIS RESEARCH, CARRIED OUT IN THE GAS TURBINE LABORATORY, M.I.T., WAS SUPPORTED BY NASA LEWIS RESEARCH CENTER UNDER GRANT NSG-3093.

FLUORESCENT VISUALIZATION FOR TURBOMACHINE RESEARCH

A. H. Epstein

MASSACHUSETTS INSTITUTE OF TECHNOLOGY
GAS TURBINE LABORATORY
CAMBRIDGE, MASSACHUSETTS 02139

MARCH 1978

FINAL REPORT 5 JANUARY 1976 - 4 JANUARY 1977

Prepared for

NATIONAL AERONAUTICS AND SPACE ADMINISTRATION
NASA LEWIS RESEARCH CENTER
GRANT NSG-3093

ABSTRACT

The quantitative gas fluorescence flow visualization technique using 2,3 butanedione as a tracer, has been refined and improved. Upgrading of the imaging system is responsible for the principal improvement. The technique has been applied to air flows in order to demonstrate its suitability to conventional compressor testing. The possibility of using butanedione to measure static gas temperature has been explored by modeling. It has been found to be feasible only when a time lag after excitation of 1 ms is acceptable.

TABLE OF CONTENTS

Section		Page
1.0	INTRODUCTION	1
2.0	ACCURACY LIMITATIONS	2
	2.1 The Illumination System	2
	2.2 The Fluorescent Gas	4
	2.3 The Imaging System	5
3.0	UPGRADING THE IMAGING SYSTEM	7
	3.1 Image Scanners	7
	3.2 Image Intensifiers	9
	3.3 System Description	10
4.0	DENSITY VISUALIZATION IN AIR	13
5.0	GAS TEMPERATURE MEASUREMENTS	14
6.0	CONCLUSIONS	20
	REFERENCES	21
	TABLE I	22
	FIGURES	23

LIST OF FIGURES

Figure		Page
1	Layout of Magnetically Focused 3-Stage Image Intensifier Camera.	23
2	Flowfield of MIT Transonic Rotor at r/r_{tip} = 0.88, M_{tip} = 1.2 (A) Image taken with old electrostatic tube. (B) Image taken with new magnetic tube.	24
3.	Fluorescent Density Visualization at r/r_{tip} = 0.88, M_{tip} =0.93 in (A) Air-Butanedione, and (B) Argon-Freon-Butanedione.	25
4.	Steady State Ratio of Intensities of Fluorescence and Phosphorescence of Biacetyl as a Function of Temperature.	26
5.	Internal Structure of 2,3 Butanedione.	27
6.	Time Response of Butanedione Luminescence for Low Levels of Illumination, Case A.	28
7.	Time Response of Butanedione Luminescence for High Levels of Illumination, Case A.	29
8.	Time Response of Butanedione Luminescence for Low Levels of Illumination, Case B.	30
9.	Time Response of Butanedione Luminescence for High Levels of Illumination, Case B.	31

1.0 INTRODUCTION

Under the sponsorship of NASA Lewis Research Center, the MIT Gas Turbine Laboratory developed a gas fluorescence flow visualization technique which yields quantitative instantaneous static density maps in a three dimensional flow field. The technique is particularly well suited for use in turbomachinery and has been used to map the flow in a rotor passage of a high work transonic rotor in the MIT Blowdown Compressor Test Facility.

The work described in this report was an effort directed at improving the overall accuracy and resolution of the quantitative density measurements, and at exploring further ways in which gas fluorescence can be used to study three dimensional flow fields.[1]

Basically the fluorescent technique consists of: 1) uniformly mixing a gaseous fluorescent tracer with the flow; 2) illuminating the seeded flow with a thin plane of laser light; 3) photographically recording the resultant fluorescent emission; and 4) computer processing the photograph to yield quantitative static density information (Fig. 1). By moving the thin incident light beam about, the three dimensional flow field of a compressor can be broken into a set of distinct and unambiguous planes. This avoids the problems that conventional interferometry and schlieren techniques have with regard to integrating out the density information along the line of sight. The fluorescent technique also yields quantitative density measurement. Quantitative measurement is extremely difficult to do with conventional techniques, even with holographic interferometry, in a geometry as complex as that of an axial flow compressor stage.

The tracer gas used in the visualization, 2,3 butanedione, was chosen because its fluorescent emission is unaffected by temperature and quenching

by foreign gas species. Thus, the emitted intensity is a function of only the incident intensity and the number of molecules in the illuminated volume, i.e. the static gas density. Because the tracer is used as a gas and is uniformly mixed with the main flow prior to the experiment, there are no problems with either uniformity of the seed or with the seed following the flow through shockwaves as there can be in particle seeded experiments.

2.0 ACCURACY LIMITATIONS

The overall accuracy of the fluorescent technique, both radiometric and spatial, is a complex function of several interrelated phenomena in both the imaging and the illumination systems. Fundamentally, however, the problem can be reduced to one of insuring sufficient signal (light) to noise level at the final detector (the photographic film). Eseentially, the degradation attributable to each step in the fluorescent imaging process can be considerably reduced at the cost of some signal (light) level. Thus, the problem becomes one of generating surplus signal level and then allocating this energy in such a way as to maximize the overall signal to noise ratio of the system.

Now let us separate the density visualization into three parts, the illumination system, the fluorescent tracer gas, and the imaging system and consider the contribution of each to the overall uncertainty of the experiment.

2.1 The Illumination System

The light source used is a 6 mm bore commercially available flashlamp pumped dye laser using Carbostyril 165 (7-dimethylamino-2-hydroxy-4-methyl-quinoline) as the dye. The laser produces a 25 millijoule pulse,

0.3 μs long at 425 nm. A dye laser had been chosen as a light source because of its large energy per pulse, ease of wavelength selection and collimated output. A dye laser is still the most attractive light source. Since the unit was purchased initally, however, the state-of-the-art of dye lasers has advanced to the point where 15mm bore units producing 250 millijoules per pulse at 425 nm are available. Cost considerations precluded purchasing a new laser.

An attempt was made to increase the energy output from the present laser by trying several newly available laser dyes and by increasing the output coupling of the laser cavity. Three new dyes were tried, Carbostyril 125,* LD425,† and LD423†. Contrary to the manufacturer's claims, LD425 did not produce an increase in output energy over the Carbostyril 165 presently used. Carbostyril 124 and LD423 both put out about 30% less energy than did the original dye.

This had been expected but it had been hoped that the dyes' shorter emission wavelength would compensate for the energy decrease by relaxing the tolerances on the laser light rejection filter on the image intensifier. The filter is necessary to keep laser light reflected from the compressor blades and casing from saturating the image intensifier (the fluorescent emission is down by 10^7 from the incident laser illumination level). These reflections have always been a problem even though the rotor was first anodized and then painted flat black. Because of the very sharp wavelength cutoff required, the interference filters used had a maximum transmission of only 50%.

---

* Manufactured by Eastman Kodak

† Manufactured by Exciton

For these reasons, it was thought that by using a dye emitting at a shorter wavelength, the increased wavelength separation between the laser output and the fluorescent emission would permit the use of a filter with an increased maximum transmission. The experimental result, however, was that the change in filter wavelength and tramission did not compensate for the reduced laser output energy.

The other attempt to increase the laser energy was to increase the output coupling of the laser cavity by replacing the 18% transmission output mirror with a 30% transmission mirror. Laser energy output is sensitive to output coupling and output increases of up to 100% have been reported with 40% output coupling.[2] In fact, however, the 30% output coupling reduced the total output energy by about 5%. The reason for this is not well understood.

The result of the above work was that there was no net increase in energy output from the flashlamp pumped dye laser.

2.2 The Fluorescent Gas

Previously, an extensive investigation[3] had revealed 2,3 butanedione to be a suitable fluorescent tracer. Although butanedione is insensitive to quenching, has a high vapor pressure, is nontoxic, and is inexpensive, butanedione has two principle drawbacks when used as a tracer. The first is that its quantum efficiency is only 0.2 %, i.e. only 0.2 % of the light absorbed by each molecule is remitted as fluorescence (the remainder goes into phosphorescence and internal photochemical processes). The second problem is that the butanedione absorption wavelengths are in the violet and ultraviolet (350-440 nm), a wavelength region in which present dye laser technology is somewhat weak. For example, the dye laser now used will emit 4-5 times more energy in the green-yellow than it will in the violet.

Although the original investigation was quite thorough, a tremendous amount of research has been done in the intervening five years on the photo-processes of organic molecules. Thus, the recent literature was searched for new fluorescent compounds. Attention was paid in particular to new laser dyes (because of their high quantum efficiency) and polymers of butanedione and related ketones.

Although several compounds with high quantum efficiency, absorbing in the right wavelengths were found none had sufficient vapor pressure to be of interest. The compounds found with the highest vapor pressure times quantum efficiency product were 4-R-1, 24-triazoline-3,5 diones (metyl and ethyl TAD).[4] These were only marginally better than butanedione, had unknown toxilogical properties, and are reportedly very difficult to synthesize. For these reasons, 2,3 butanedione was retained as the fluorescent tracer.

2.3 The Imaging System

The original imaging system used photographic film to record the output of a 3-stage electrostatically focused image intensifier. The 25 mm diameter tube had an S-20 photocathode. The tube's fiberoptic output and grounded anode permitted the use of contact photography. Thus no light was lost in a relay lens. While the tube has a high gain, its principle advantage was its low cost (since it was in mass production for the military).

Unfortunately, the electrostatic image intensifier has several limitations which impacted severely on the accuracy of the fluorescent density measurements. The three principle problems are geometric distortion, gain variation over the tube face, and internally generated noise.

The tube's pincushion geometric distortion stemmed from limitations in the design of the tube's electrostatic focusing lenses. The result is that

the tube's geometric magnification is proportional to the square of the radial displacement from the optical center of the tube. Thus, this effect is most noticeable near the periphery of the image. Since the distortion proved to be stable with time and tube gain, most of the resultant error could be calibrated out.

The radiometric gain varies over the face of the tube by a factor of 3 to 1. This variation results from both the electron optics and phosphor nonuniformities. The variation was also stable with time and gain and thus could be allowed for in calibration. Note, however, that the required correction is quite large (300%) compared to the final radiometric accuracy required for the gas density measurements (~3%).

The most important source of imprecision in the electrostatic tube is tube noise. This noise coming principally from the first stage photocathode, has a characteristic spatial extent on the order of 300 microns. Please note that the equivalent input noise of a particular tube is essentially fixed and therefore independent of the gain at which the tube is operated. Thus, the signal to noise ratio (SNR) is established by the level of the signal from the experiment. In this case, the SNR was about 4 to 1.

Since only one image of the flow can be made at a given time, the noise cannot be averaged out over several exposures as is often done with low light level imaging. In this case, the only way the noise level of a particular tube can be reduced is to spatial average over the image, thus trading spatial resolution for SNR. The averaging has an additional affect in that it restricts the limiting of the image to the central portion of the tube to minimize geometric distortion and gain variation because the final spatial resolution would be insufficient for the experiment.

Thus, the image tube imperfections and, in particular, image tube noise is a major contributor to gas density uncertainty.

3.0 UPGRADING THE IMAGING SYSTEM

A very wide variety of imaging devices and recorders were examined in detail. These can be divided into two general categories, scanning devices with electronic readout (vidicons for example) and whole imaging devices, principally various types of image intensifiers. The devices were evaluated with respect to gain, radiometric resolution, geometric fidelity, geometric resolution, long-term stability, and overall signal to noise ratio.

3.1 Image Scanners

Considerable time was spent exploring various low light level T.V. type imaging systems. Particular attention was paid to silicon intensified target (SIT), intensified silicon target (ISIT), intensified vidicon, secondary electron conduction (SEC), and intensified SEC (ISEC) tubes. All of these tubes have sufficient gain for the gas fluorescent measurements, (although the gain of some of the unintensified tubes is somewhat marginal.) The SNR of commercially available camera systems using these tubes ranges $32 \sim 40$dB. The gamma * (γ) of the tubes are in the $0.7 \sim 0.9$ range.

A common requirement of the T.V. type imaging devices is the need to record or buffer the output for later digitization. Recording devices considered include video tape, video disc, scan converters, and direct digital

---

* Gamma is the slope of the ratio of the log of output to the log of input $\gamma = \tan \frac{\log Eout}{\log Ein}$ and is thus a measure of the device's relative resolution.

converters and buffers. Video tape and discs were rejected because the only units with sufficient SNR cost between $30,000 and $50,000 (units for commercial broadcasting.) Direct digital conversion was rejected because there was not a computer available to accept the high bandwidth input.

The device which seemed the most suitable was the scan converter. Scan converters accept single frame inputs at standard T.V. framing rates and formats, store the inputs for times ranging upward of 10 minutes, and can non-destructively output the stored information at an arbitrarily slow data rate. There are two types of scan converters, differing primarily in how the information is internally stored. Analogue units employ a storage tube which is, in concept, a combined CRT and vidicon. These devices typically have SNR's of 40-42dB (a principal noise source is the video preamplifier) and cost $4,000 - $6,000.

Digital scan converters consist of a very high speed analogue to digital converter and solid state memory. Readout can be either in direct digital form or converted back to analogue signals. The SNR of digital scan converters can be higher than that of the analogue types (up to 48dB) but the digital versions cost 2 to 4 times as much. Thus, a T.V. type imaging system including a scan converter storage can have an overall SNR of 40dB.

New generations of solid state diode type arrays are continually appearing on the commercial market. The solid state arrays offer the advantage of low complexity and relatively low cost. When cryogenically cooled, commercially available devices have demonstrated 80dB usable radiometric resolution.[5] Unfortunately, the units which are presently commercially available lack the sensitivity in the 0.45 micron wavelength region that is necessary for butanedione fluorescence measurement.

Units with enhanced ultraviolet response have been demonstrated and may be usable in the near future.

3.2 Image Intensifiers

Image intensifiers were extensively surveyed with respect to SNR, gain, distortion and resolving power. The principal source of noise in an image intensifier is the dark emission from the photocathode. This thermal emission can be traded off against the red response of the phosphor. Fortunately, butanedione emission is at short wavelength (0.45 microns). Thus, a blue response bialkali photocathode was chosen over the standard extended range multi-alkali S-20 type in the original electrostatic tube.

Although some consideration was given to using the center portion of a large area (90-140 mm dia) electrostatically focused tube, the large tubes' high cost (~$50,000) reduced their attractiveness. Magnetically focused tubes seemed better suited for this application because of their superior SNR and low distortion. The magnetic tube's principal disadvantage is its much greater complexity, due to the required focusing magnet and auxiliary equipment.

Careful consideration was made of the advantage of an image intensifier versus a T.V.-type electronic readout imaging system. The T.V. system's greatest advantage is its elimination of photographic film, one of the weakest quantitative links in the fluorescent gas measurement. Another advantage is its nearly instantaneous readout and data processing input, as opposed to the film development and subsequent scanning necessary with the photographic system.

The greatest advantage of the image intensifier-photographic film system is its high resolution. Although the film may not be as quantitative as direct electrical readout, the photographs contain a great deal of qualitative

information for the aerodynamicist which may be lacking in the lower resolution T.V. images. An addition factor is the cost. A complete T.V.-type imaging and recording system can be twice as expensive as an image intensifier of equivalent gain and SNR.

3.3 System Description

On the basis of the above, a magnetically focused image intensifier was selected as the imaging device. The particular tube chosen (an EMI Model 9914) was selected because of its lower noise level and price compared to competitive types. The tube is a 38 mm diameter, 3 stage, electro-magnetically focused intensifier with a bialkali photocathode and glass input and output windows. The tube has provisions for electronic gating(1 microsecond exposure time) but this feature was not used in the present experiment.

The image intensifier was equipped with an 85 mm f/1.2 objective lens (geometric constraints imposed by the tube focusing magnet prevented the use of a larger aperture.) This objective lens is capped by an electromagnetic shutter.

A glass faceplate and relay lens (as opposed to fiberoptic output and contact photography) were chosen for two reasons. The first is relay lens spacing allowed the placement of a fast (10 millisecond) electromagnetic shutter in the output optical path. This shutter serves to prevent exposure of the film to tube noise except during the short (20 ms) period around the laser firing. The second reason is that the output screen's location within the focusing coil would make contact photography mechanically difficult. The 85 mm f/1.0 relay lens is normally used at an aperture of f/1.4 or f/2.0 to reduce spherical aberration. The image intensifier layout is shown in Fig. 1.

The performance of both the old and new image intensifiers are compared in Table 1. Note that the geometric distortion, gain variation and dark noise are dramatically improved, as are the resolution and useful area.

The principal problem encountered with the new image intensifier was that, due to the factor of 50 light loss in the relay lens and brightness limitations on the output phosphor, the film used with the old contact image intensifier no longer had sufficient sensitivity. This was unfortunate since the film, Kodak Contrast Process Ortho Type 4154, was very well suited to the gas density measurements because of its fine grain and high gamma ($\gamma = 3$). The high gamma means that, with an 8-bit (1 part in 256) film scanner, as density variations on the order of 2% can be measured.

Type 4154's marginal sensitivity was known before the new image tube was selected and a film with an equally high gamma but increased sensitivity, Kodak Linagraph Ortho, had been selected as a replacement. Unfortunately, Linagraph Ortho was withdrawn from the market about the time the new tube was delivered. The replacement recommended by the manufacturer did not have as high a gamma. After a very extensive literature search, conversations with photographic film manufacturers, and some darkroom experimentation (trading increased development and gamma for a higher fog level and granularity), an aerial film, Kodak Plus-X Aerographic SO 2402, was chosen as having the most suitable gamma-granularity tradeoff. Note that this gamma is about 1.8 - 2.0. Because the exposure and development are very closely controlled, the maximum photographic film density (corresponding to the highest gas density) can be kept within narrow tolerances. By reducing the maximum exposure (film density) as compared to that used with the old tube, the film scanner can be used on a more sensitive scale, thus compensating for the

reduced gamma of the new film. Thus, little is lost quantitatively with the new film. However, photographic prints of the negatives appear somewhat less sharp to the unaided eye.

The only other problem with the new image intensifier is that it is somewhat more difficult to use than the old one. The old tube only required an input operating voltage of about 6 volts (a miniature high voltage power supply was packaged within the tube envelope). Its gain was proportional to the input voltage. No other adjustment was necessary or possible. The new magnetically focused tube required a 30 kV high voltage supply, a 20 amp low voltage supply for the focusing magnet, and careful cooling. Focusing of the device requires adjustment of the high voltage, of the relative potential across each of the three stages, and adjustment of the focusing coil field strength -- a somewhat tedious procedure.

A comparison of the performance of the old and new image tube is shown in Fig. 2. The image is of the flow in the MIT transonic rotor at a hub-to-tip ratio of 0.88. The magnetically focused tube product is one of considerably less noise and of increased resolution. Also, the large variations in tube gain and geometric distortion are no longer evident. There are some differences in the flow field since the picture with the old tube was taken with the rotor operating alone. The flow imaged by the new tube was of the complete stage. The entrance to a stator passage can be seen as the two bright dots at the upper left of Fig. 2b.

Although not quite ideal, the new imaging system represents the principal upgrading of the gas fluorescent density measurements.

4.0 DENSITY VISUALIZATION IN AIR

The MIT Blowdown Tunnel uses an Argon-Freon mixture as the working gas in order to minimize the mechanical rotation speed necessary for a given rotor tip Mach number. All work with 2,3 butanedione fluorescence has been done with this mixture. In order to demonstrate the fluorescence technique's compatibility with conventional mixture to ensure (a) that butanedione fluorescence is not quenched by oxygen and (b) that the air-butanedione mixture useful for fluorescence experiments will not detonate.

Quenching was not thought to be a problem since, although butanedione phosphorescence is strongly quenched by oxygen, the short lifetime fluorescence does not have this problem. In fact, butanedione visualization in air had previously been demonstrated on a small scale ballistic tube experiment.[1]

Safety, however, could be a severe problem in a conventional test rig because of possible detonation and fire. The only information reported in the literature on this point is that 2,3 butanedione has a flash point of 70°F in air. A simple stochiometry calculation showed, however, that at the 2% molar concentration used in the gas fluorescence experiment, butanedione flammability should not be a problem. Nevertheless, the MIT Blowdown Tunnel is a nearly ideal facility to experiment with since (a) the tunnel walls are thick enough to withstand an air-butanedione explosion; (b) the tunnel is itself located in a concrete blast cell; and (c) the detonation of the 2.5 grams of plastic explosive used to rupture the diaphragm at the start of each test would probably initiate any possible detonation of the gas mixture.

Five blowdown tests were run with a mixture of 480 mmHg of air and 20 mm of butanedione with no evidence from either pressure transducers or surface deposits of detonation or burning of the mixture. Four of these tests were run with an initial total gas temperature of 212°F.

Fluorescent images (Fig. 3) were taken at the same tip Mach number (M_T = 0.90) and radial position (r/r_T = 0.88) in both air-butanedione and Argon-Freon butanedione mixtures. (The tip Mach numbers were limited by mechanical rotational speed constraints.) In both cases, the flow fields are qualitatively similar with the only differences being the normal shot-to-shot variations in a transonic flow. Unfortunately, some of the auxiliary blowdown tunnel instrumentation was removed so it is not clear that the stage is operating at exactly the same point on the map.

The intensity of the butanedione fluorescence was the same in the air mixture as in the Argon-Freon mixture. The conclusion is that butanedione gas fluorescence density visualization is as practical in air as in an Argon-Freon mixture.

5.0 GAS TEMPERATURE MEASUREMENTS

Many variations on the gas fluorescence density visualization may be feasible. One of the potentially most useful extensions of the present technique would be the direct, quantitative measurement of static gas temperature in a transonic flow using butanedione luminescence. This idea is suggested by past studies by Okabe and Noyes[6] which show that in the steady state the ratio of intensities of butanedione fluorescence (blue) to butanedione phosphorescence (green) is strongly temperature dependent (Fig. 4).

Basically, the fluorescent quantum efficiency is temperature independent while that of the phosphorescence varies exponentially with temperature. Thus, temperature can conceivably be measured with just a measurement of the relative emission intensities in the blue and the green. This is convenient since relative light intensities are much easier to measure than are

absolute values. If the absolute value of the blue fuorescent emission is simultaneously measured, then the static gas density is determined as well.

Unfortunately, the data presented in Fig. 4 is the total information in the literature on butanedione emission temperature sensitivity. Before proceeding with any flow experiment, an attempt was made to better understand the role temperature plays in the internal photoprocesses of 2,3 butanedione.

In particular, there was some concern that the slow time response of the phosphorescence (1 millisecond) might prove limiting to the process.

The mathematical model described in Ref. 3 was modified to include the effect of phosphorescent temperature sensitivity. This is prefaced by a short review of butanedione photoprocesses.

Luminescent molecules, like butanedione, can be described by an energy level diagram (Fig. 5). S_0 is the ground state. S_1, S_2, S_3, ---S_n are the excited singlet states. T_0, T_1, T_2...T_n are the excited triplet states. The decay rates of the upper singlet states ($S_n -> S_1$) and the upper triplet states ($T_n -> T_0$) are extremely fast. This means that the behavior of these upper states can be ignored. Thus, the excited singlet states are modeled as one singlet state S_1 and the excited triplet states are modeled as one triplet state T_0. Therefore, we are left with a three level system: ground state S_0, singlet state S_1 and triplet state T_0.

The behavior of a three-level system is characterized by the electron population of each energy level. The electron population is determined by the transition rates from one energy level to another. In this model, there are five tramsition rates that are of interest.

k_S = non-radiative decay rate from S_1 to S_0

k_F = radiative decay rate from S_1 to S_0

k_{ST}= intersystem crossing rate from S_1 to T_0

k_T = non-radiative decay rate from T_0 to S_0

k_P = radiative decay rate from T_0 to S_0

The blue luminescence at 460 nm is the fluorescence. Fluorescence is due to the radiative decay from the excited singlet state S_1 to ground state S_0. The green luminescence at 510 nm is the phosphorescence. Phosphorescence is due to the radiative decay from the excited triplet state T_0 to the ground state S_0.

From past experimental results, one obtains the following rate equations.

$$\frac{I_P}{I_F} = \frac{k_{ST}}{k_F}\cdot\frac{k_P}{k_P+k_T} = f(T) \quad \text{where} \quad (T)\ 1.63\times10^{5}e^{-0.025T}$$

T = temperature ^{o}K

$$\frac{I_P}{I_0} = \frac{k_F}{k_{ST}+k_F+k_S} = C_1 \quad \text{where } C_1 = \text{constant} = 0.0025$$

$$\tau_S = \frac{1}{k_{ST}+k_F+k_S} \quad \text{where } \tau_S = \text{excited singlet state lifetime} = 10^{-8}\text{sec}$$

$$\tau_T = \frac{1}{k_P+k_T} \quad \text{where } \tau_T = \text{excited triplet state lifetime}$$

Unfortunately there are only four equations and five unknown transition rates. Another equation is needed. The fifth equation can be obtained by a simplifying assumption. We will consider two possible assumptions. The first assumption is that electron transitions due to non-radiative decay from the singlet state are negligible compared to fluorescence and intersystem-crossing (i.e. k_F, $k_{ST} >> k_S$). Call this case A. The other assumption is that the electron transitions due to the non-radiative decay from the triplet state are negligible compared to the

phophorescence (i.e., $k_P >> k_T$). Call this case B. Using these assumptions, two sets of transition rates were formulated. For k_F, $k_{ST} >> k_S$, the transition rates are the following:

$$k_{ST} = \frac{1-C_1}{\tau_S} \quad k_F = \frac{C_1}{\tau_S} \quad k_S << k_F$$

$$k_P = C_2 \qquad k_T = C_2\left(\frac{1-C_1}{C_1 f(T)} - 1\right)$$

where from experimental results:

$$C_1 = 0.0025$$

$$C_2 = 83.5$$

$$\tau_S = 10^{-8} \text{ sec}$$

$$f(T) = 1.63 \times 10^{+5} \exp(-0.025T)$$

$$T = \text{temperature } {}^{o}K$$

For $k_P >> k_T$, the transition rates are the following:

$$k_{ST} = \frac{C_1 f(T)}{\tau_S} \quad k_F = \frac{C_1}{S} \quad k_S = \frac{1-C_1(f(T)-1}{\tau_S} \quad k_P = \frac{1}{\tau_T} \quad k_T << k_P$$

where $\tau_T = 10^{-3}$sec

In order to obtain the time response of the fluorescence and phosphorescence to incident radiation I_0, each set of transition rates were substituted into the butanedione rate equations from Ref. 3.

$$\frac{I_F}{I_0} = \frac{P}{(\beta-\alpha)}\left[\left(1-\frac{L}{\alpha}\right) e^{-\alpha t/\tau_S} + \left(\frac{L}{\beta}-1\right) e^{-\beta t/\tau_S} + \frac{L(\beta-\alpha)}{\alpha\beta}\right]$$

$$\frac{I_P}{I_0} = \frac{PR}{\alpha\beta(\beta-\alpha)}\left[\alpha e^{-\beta t/\tau_S} + \beta e^{-\alpha t/\tau_S} + (\beta-\alpha)\right]$$

where

$$\alpha = \sqrt{\frac{L+Q}{2} - \frac{1}{2}(L+Q)^2 - 4(SR-LQ)}$$

$$\beta = \sqrt{\frac{L+Q}{2} + \frac{1}{2}(L+Q)^2 - 4(SR-LQ)}$$

$$L = \tau_S/\tau_T$$

$$R = \tau_S k_{ST} k_P/k_F$$

$$P = k_F\tau_S\left(\frac{C_0 0 N_0}{h\nu}\right) + 1$$

$$Q = \frac{I_0 0 \tau_S}{h\nu} + 1$$

$$S = \frac{I_0 0 \tau_S}{h\nu} - \frac{k_F}{k_P}$$

I_0 = incident intensity

I_P = phosphorescence intensity

I_F = fluorescence intensity

0 = absorption cross section

$= 6.4 \times 10^{-20}$ csn^2

$h\nu$ = incident photon energy

$= 4.6 \times 10^{-19}$ joules

Figure 6 shows the calculated ratio of I_P to I_F as a function of gas temperature for case A (k_F, $k_{ST} >> k_S$) for a step light input. In this case, the phosphorescence transition rate is limiting. Therefore, the emission ratio is temperature independent until approximately 1 millisec. after the start of the light pulse. In a 300 meter per second flow, this is an unacceptable time lag. Because the rate at which the lower triplet state is pumped is dependent on the incident intensity (I_0) - for high levels of I_0 -, the results in Fig. 6 were recalculated with I_0 increased by a factor of 10^4. Figure 7 shows that the rise time of the emission has increased by only a factor 2. This is still too slow for use in a transonic flow.

The time response for assumption B is shown in Fig. 8. In this case, the response is no longer limited by the phosphorescent rate constant so that the ratio of intensities essentially follows the growth of the phosphorescent level. This case is also sensitive to the magnitude of I_0, so Fig. 9 shows the rise time for assumption B with an increase in incident intensity of 10^4. In this case, the rise time has increased by an order of magnitude. The response time of case B is fast enough for use in a transonic flow field.

The question remains which set of calculations is the correct model. This can be answered by examining the transition rates. For a small non-radiative triplet decay rate, the intersystem crossing rate decreases with an increase in temperature:

$$k_{ST} = \frac{C_1 f(T)}{\tau_S} \propto e^{-0.025T}$$

For a small non-radiative triplet decay rate increases with temperature:

$$k_T = C_2 \frac{1 - C_1}{C_1 f(T)} \propto e^{+0.025T}$$

It seems more likely that the non-radiative triplet decay rate increases with temperature because of increased collisions and collisional de-activation at higher temperatures due to higher translational energy. This is supported by recent studies on similar molecules such as Methyl TAD. Whereas, there is no readily apparent temperature dependent mechanism that is capable of significantly changing the intersystem crossing rate k_{ST}. Therefore we believe that the correct butanedione model is the one that assumes a negligible non-radiative decay rate, case A.

The MIT Blowdown Compressor operates with an 82% Argon and 18% Freon gas mixture that has a sonic velocity of about 250 m/sec. Thus, for a transonic flow, the butanedione mixed in with the Argon and Freon will travel a distance of 0.25 m beyond the point of initial temperature excitation before any significant change in the fluorescence-phosphorescence intensity ratio can be detected. This is clearly unacceptable. For this reason, no further work has been done on butanedione temperature measurement.

6.0 CONCLUSIONS

The gas fluorescence density visualization technique has been upgraded, principally by replacing the original electrostatic image intensifier camera with a higher performance magnetically focused device. This improvement has been demonstrated with flow visualization of the flow field in the MIT Blowdown Compressor.

The fluorescent technique has also been applied to air in order to demonstrate its suitability for conventional compressor test stands. The technique has been shown to work in air and no problems with flammability were encountered.

The possibility of using 2,3 butanedione luminescence to measure gas static temperature has been explored by modeling the internal structure of the molecule. The results of the model show that although butanedione luminescence can be a sensitive measure of temperature, its frequency response is only of the order of 1 kHz. This is too low for use in a high speed turbomachine.

REFERENCES

1. Epstein, A. H., "Quantitative Density Visualization in a Transonic Compressor Rotor," Ph.D. Thesis, Aero & Astro, M.I.T., Sept. (1975).

2. Neister, E., Phase-R Corp., private communication.

3. Epstein, A. H., "Fluorescent Gaseous Tracers for Three Dimensional Flow Visualization," S.M. Thesis, Aero & Astro, M.I.T., June (1972).

4. Pocius, A. V., and Yarolly, J. T., "Intramolecular Energy Transfer in 4-R-1,2,4-Triazoline-3,5-Diones: Relation to Theory and Photochemical Reactivity," J. Chem. Phys. 61, 2779 (1974).

5. Madejski, G., Smithsonian Astrophysical Observator, private communication.

6. Okabe, H., and Noyes, W. A., "The Relative Intensities of Fluorescence in Biacetyl Vapor," J. Am. Chem. Soc. 79, 801 (1957).

TABLE 1

IMAGE INTENSIFIER PERFORMANCE

	Magnetic Tube	Electrostatic Tube
No. of Stages	3	3
Image Diameter (mm)	38	24
Center Resolution (lp/mm)*	48	36
Radiant Power Gain (max)*	200,000	88,000
Geometric Distortion*	2%	14%
Spatial Variation in Gain*	± 15%	± 150%
Noise (cm^2) Equivalent Background Input*	5×10^{-15}	1.6×10^{-11}

* Measured for Gas Turbine Laboratory tubes.

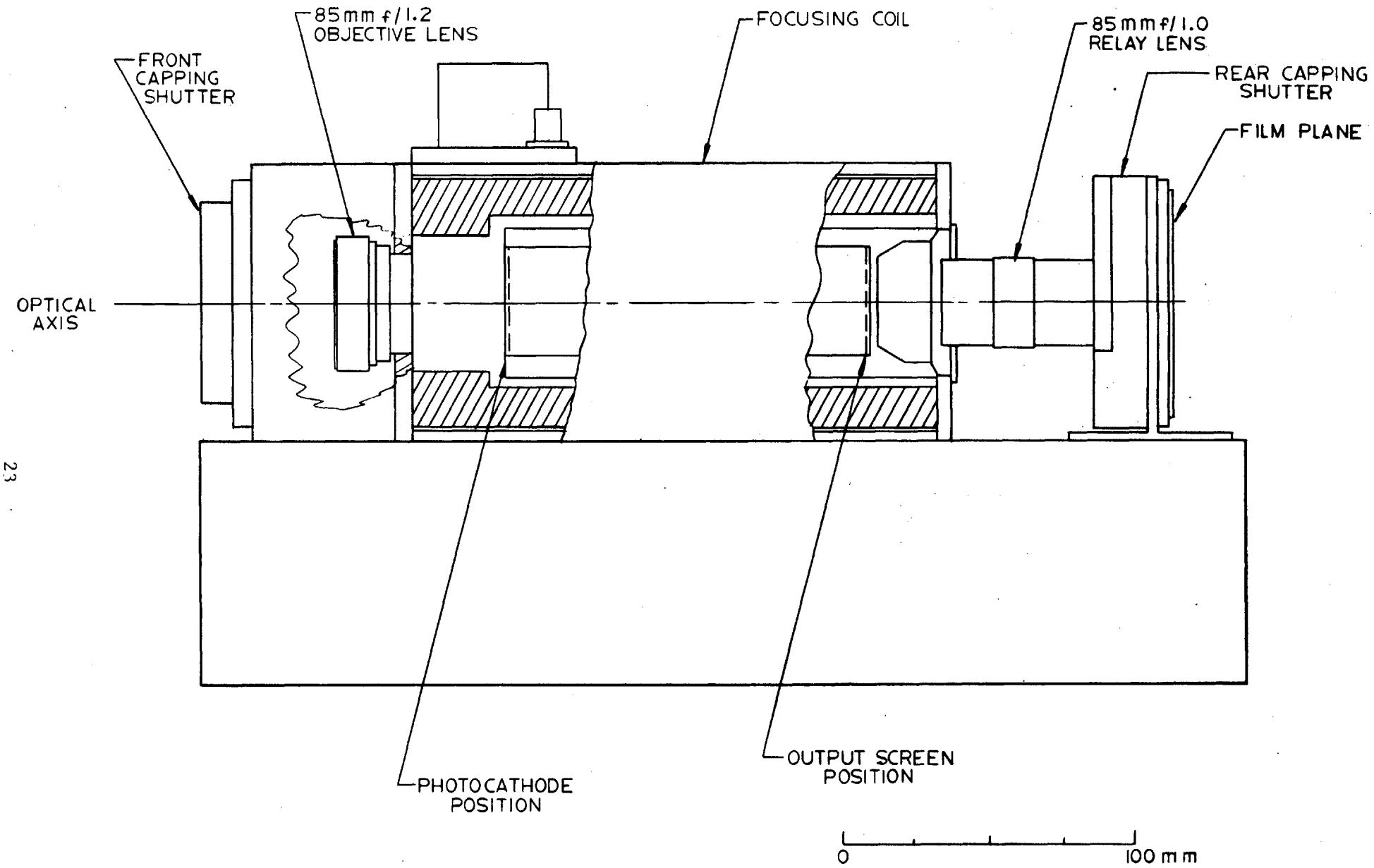

FIGURE 1: LAYOUT OF MAGNETICALLY FOCUSED 3-STAGE INTENSIFIER CAMERA.

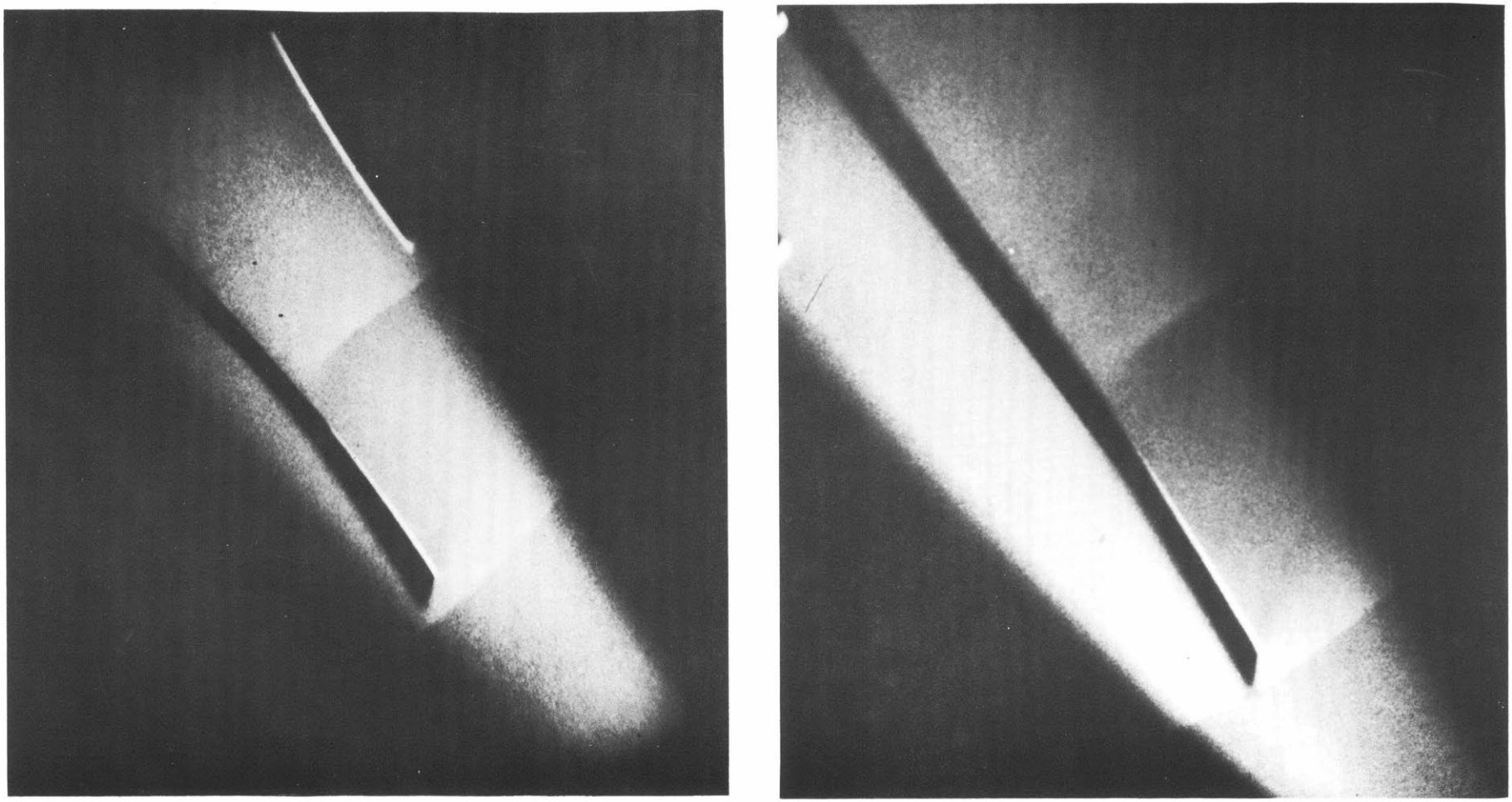

(A) Image taken with Old Electrostatic Tube. (B) Image taken with New Magnetic Tube.

Figure 2: Flowfield of M.I.T. Transonic Rotor at r/R_{TIP}= 0.88, M_{TIP}= 1.2.

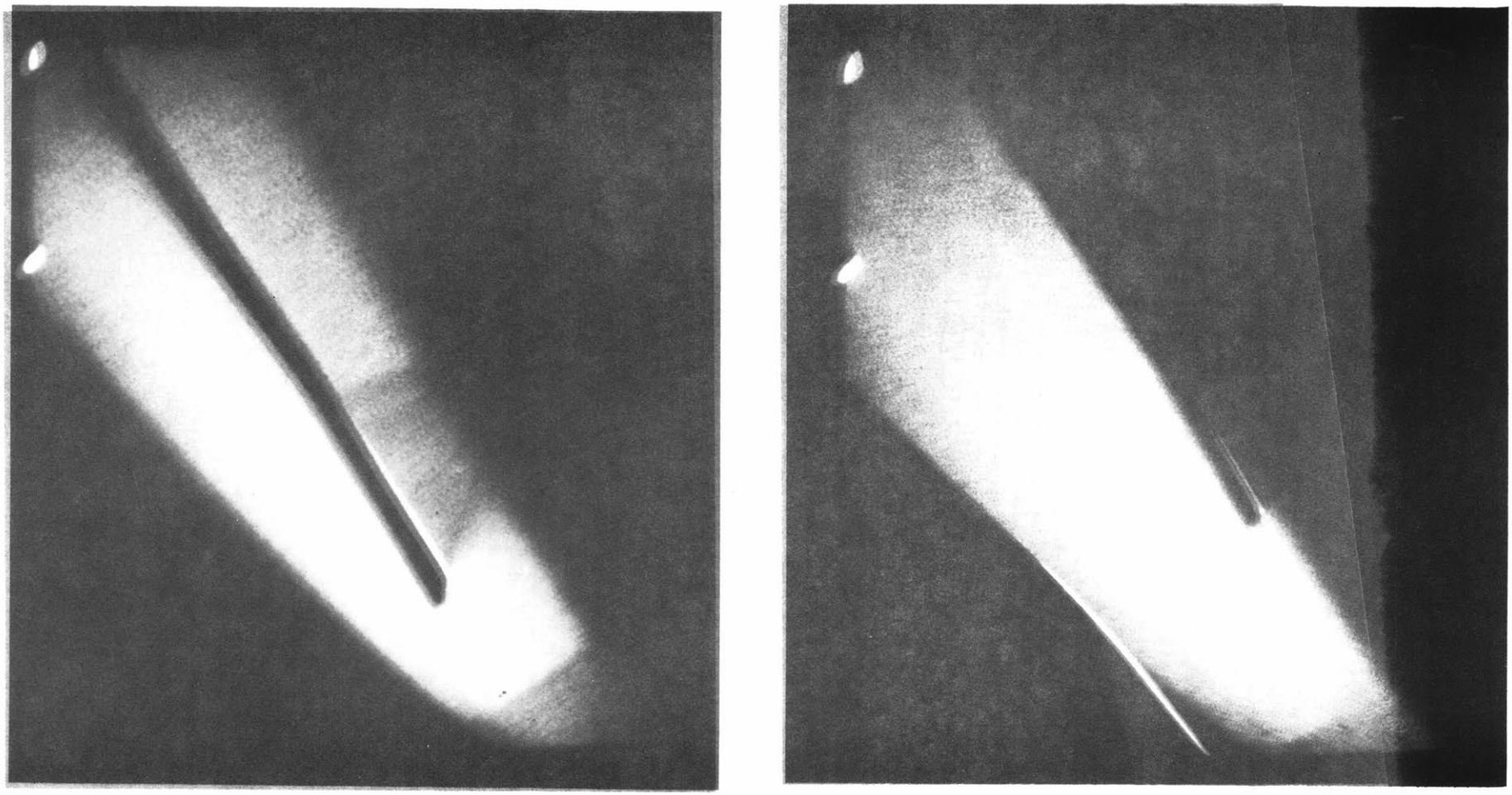

(A) (B)

FIGURE 3: FLUORESCENT DENSITY VISUALIZATION AT $R/R_{TIP} = 0.88$, $M_{TIP} = 0.93$ IN (A) AIR-BUTANEDIONE, (B) ARGON-FREON-BUTANEDIONE.

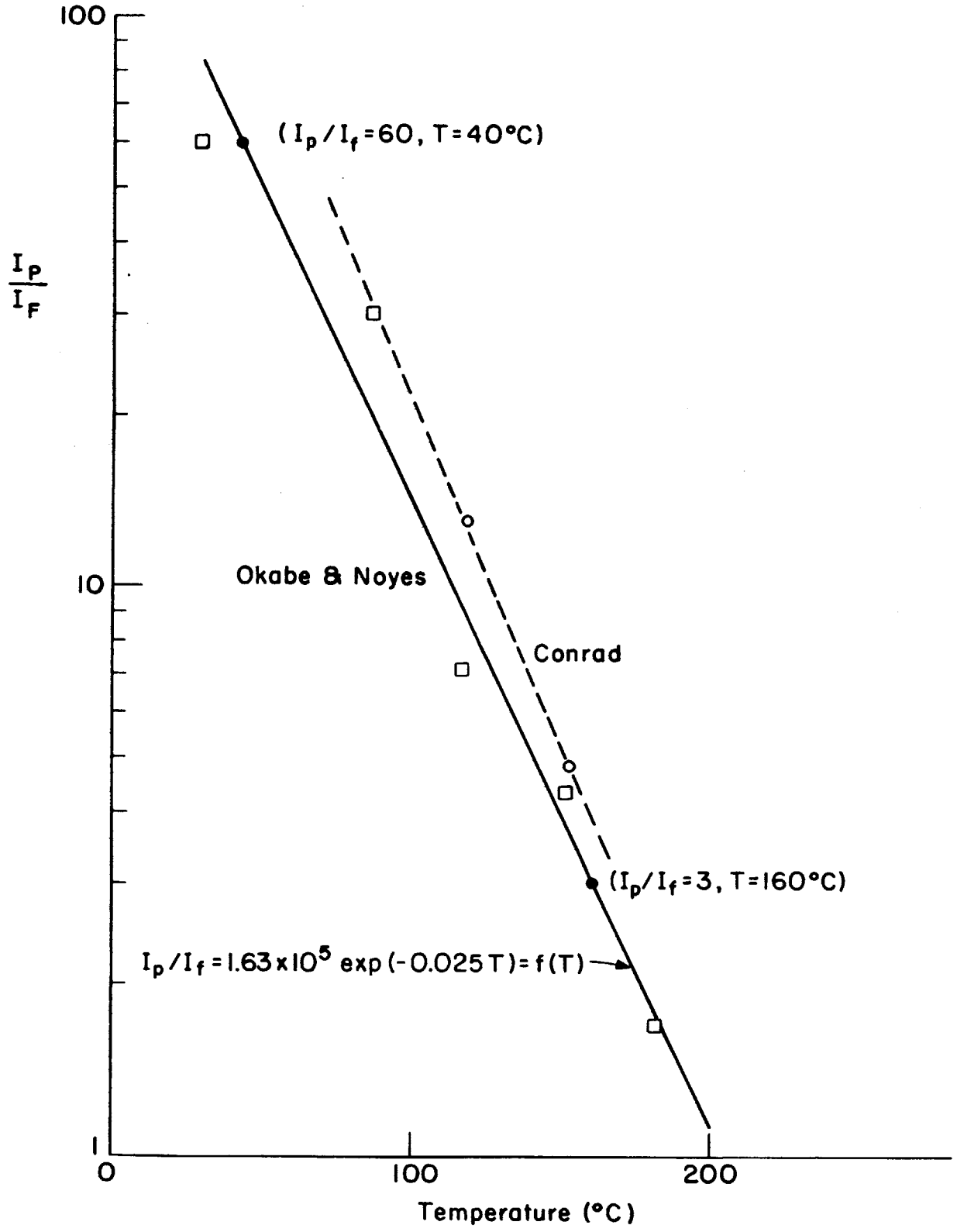

FIGURE 4: STEADY STATE RATIO OF INTENSITIES OF FLUORESCENCE AND PHOSPHORESCENCE OF BIACETYL AS A FUNCTION OF TEMPERATURE.

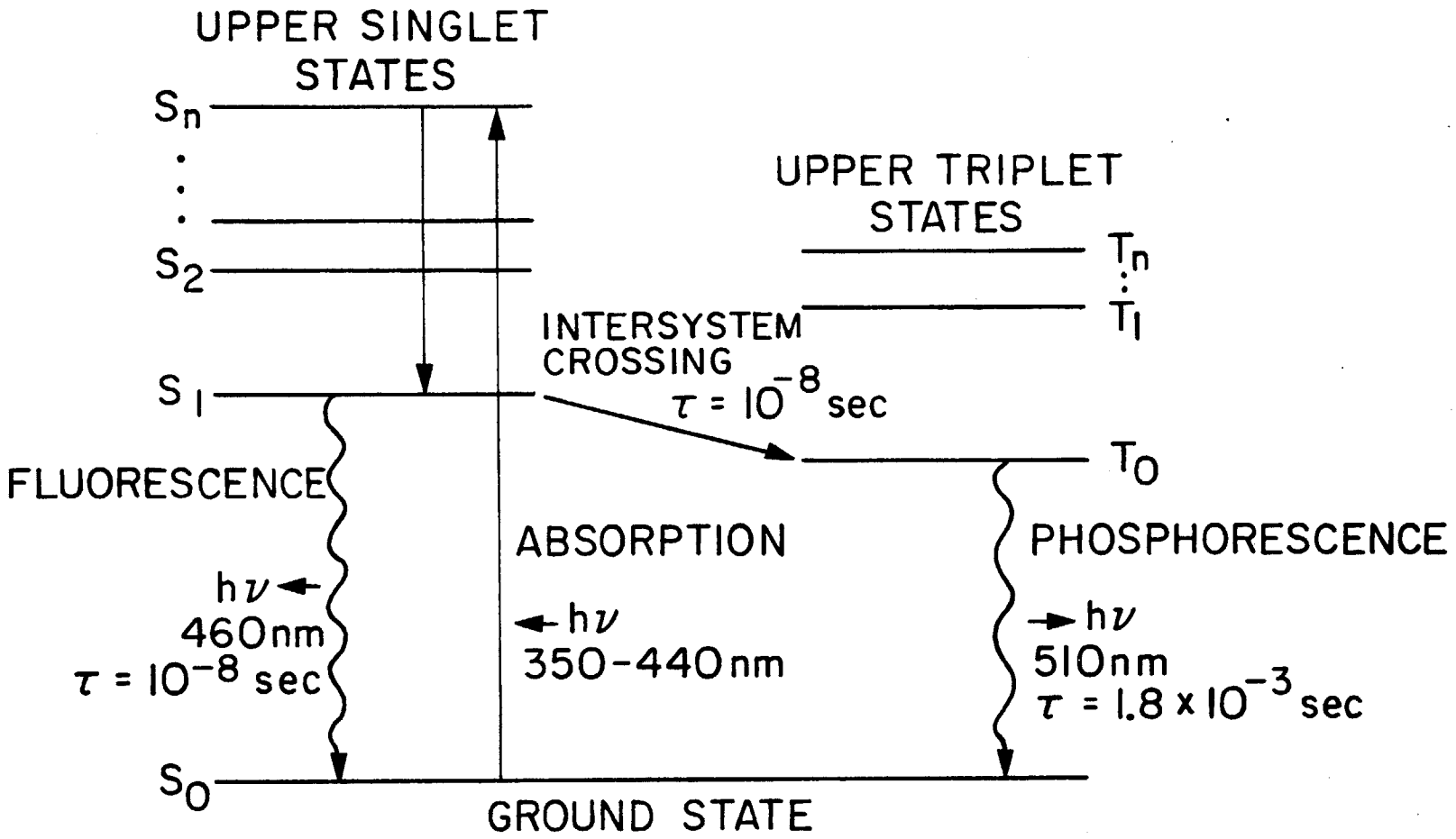

FIGURE 5

INTERNAL STRUCTURE OF 2,3 BUTANEDIONE ($CH_3COCOCH_3$)

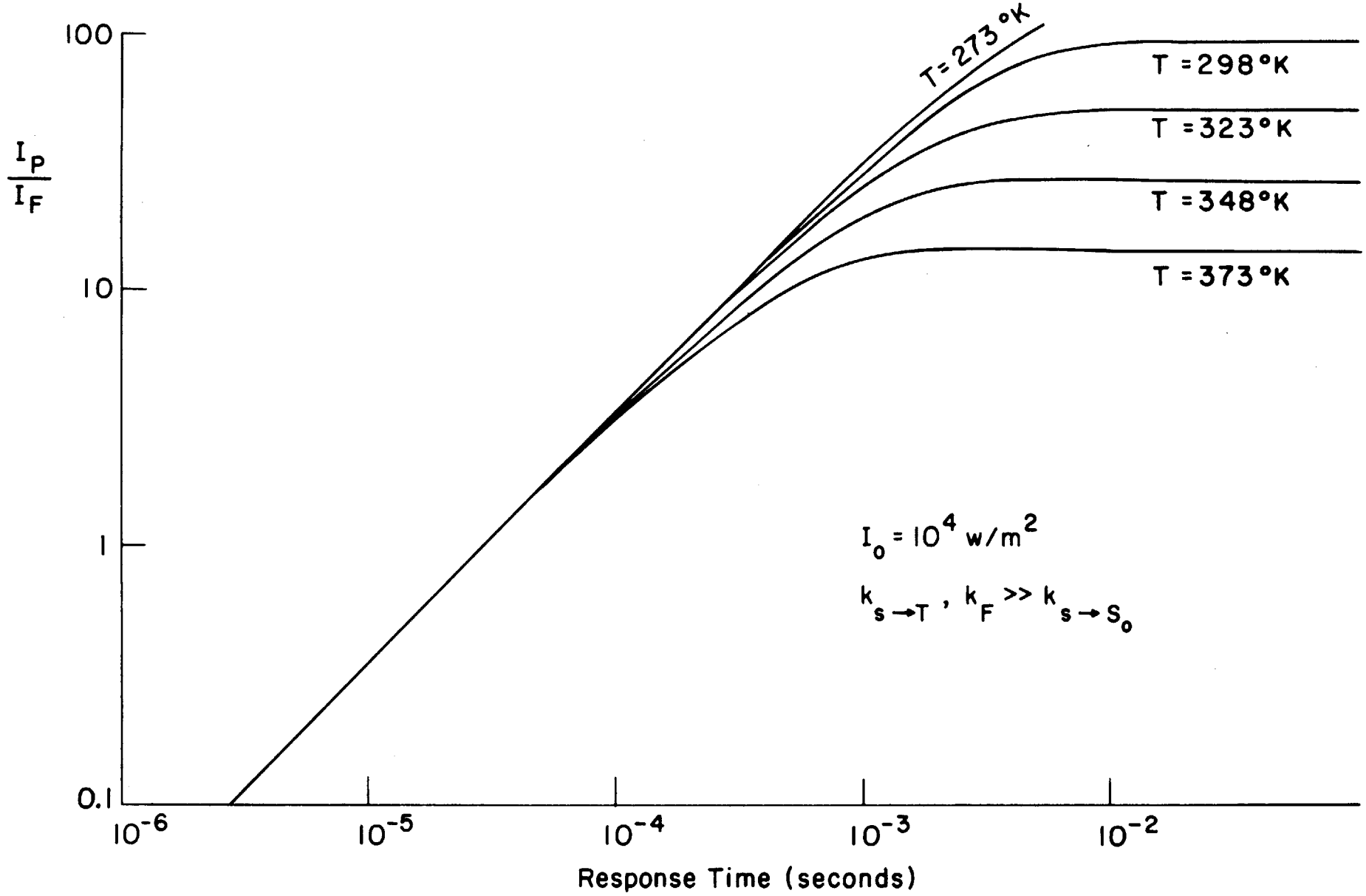

FIGURE 6: TIME RESPONSE OF BUTANEDIONE LUMINESCENCE FOR LOW LEVELS OF ILLUMINATION, CASE A.

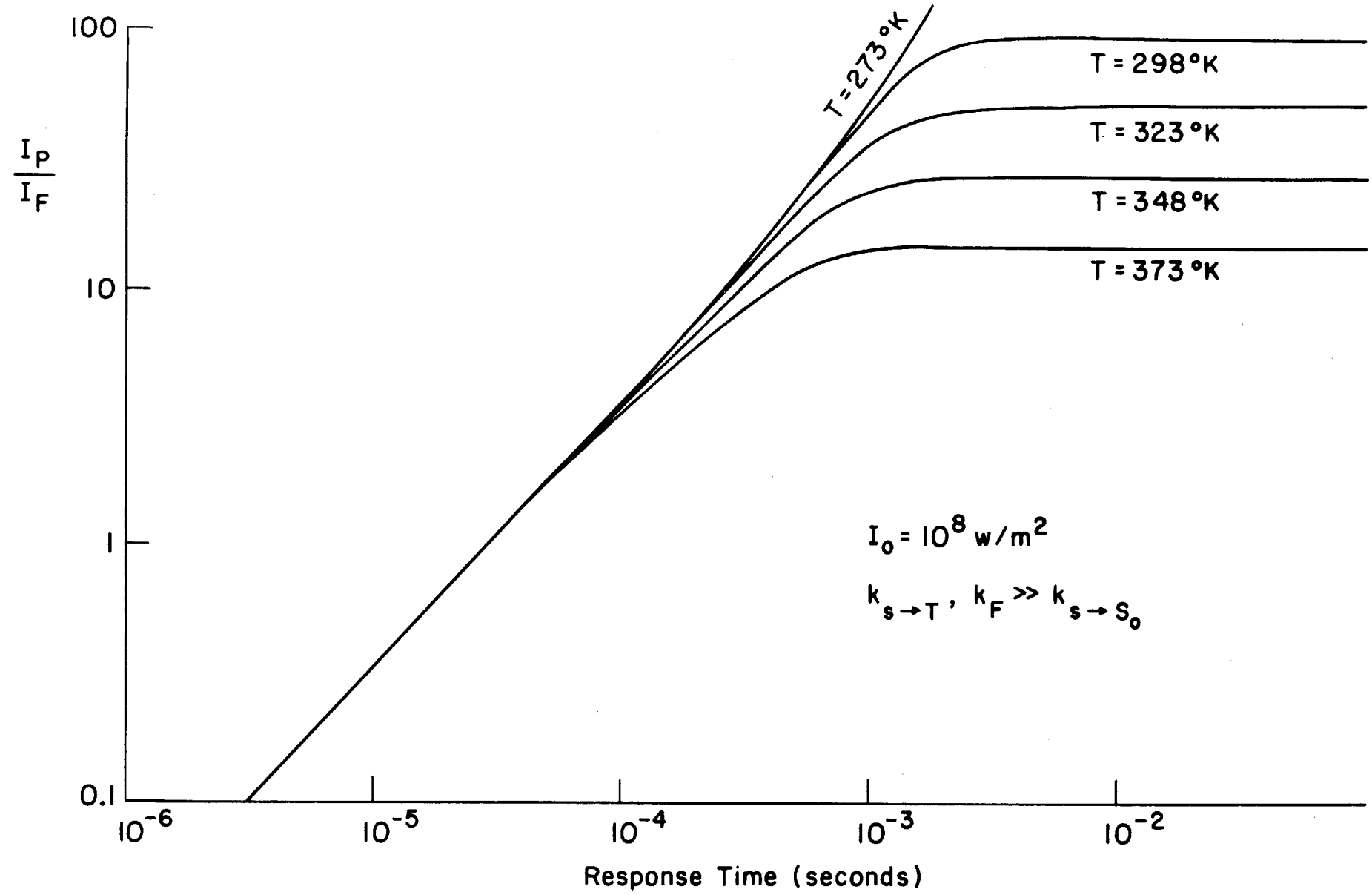

FIGURE 7: TIME RESPONSE OF BUTANEDIONE LUMINESCENCE FOR HIGH LEVELS OF ILLUMINATION, CASE A.

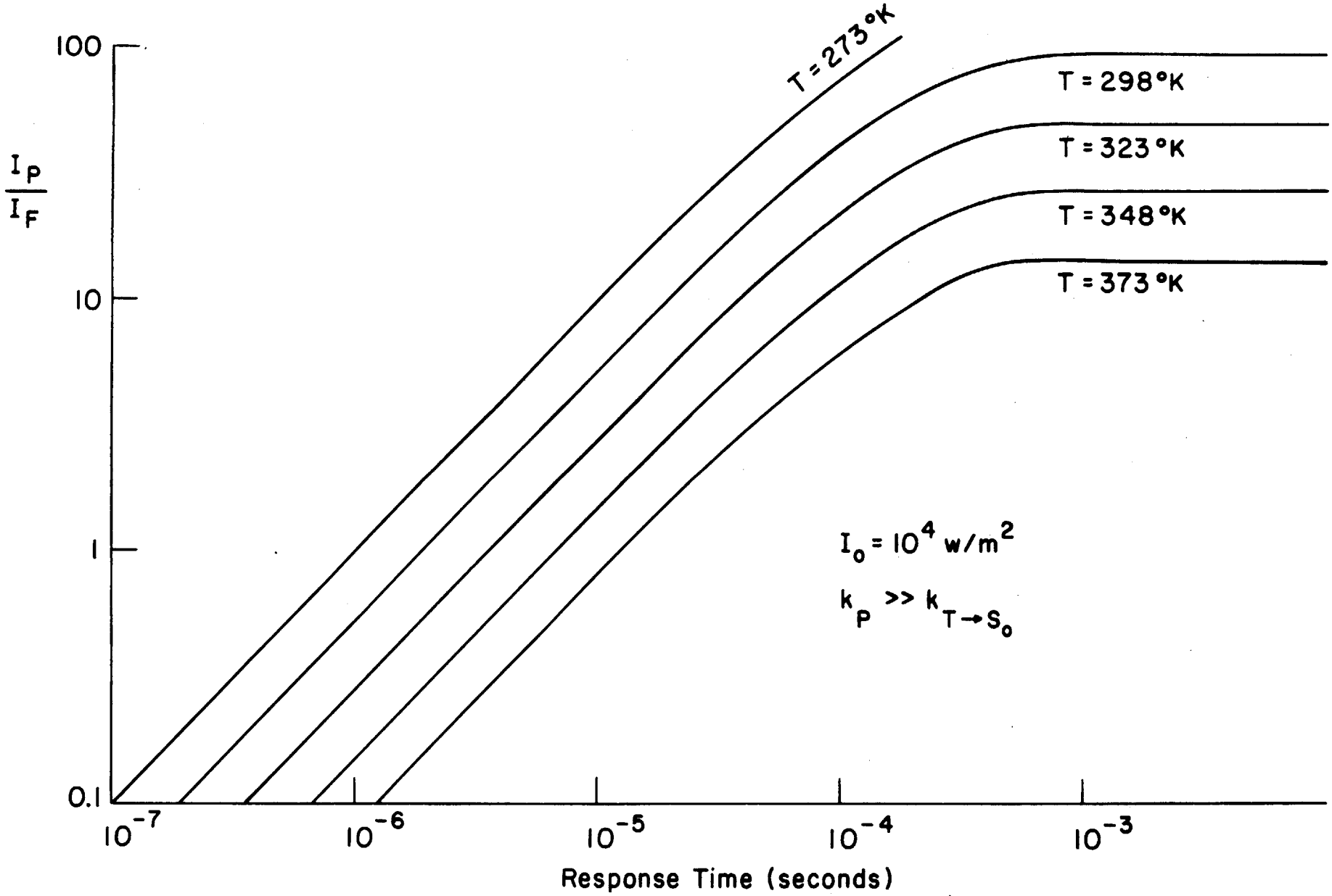

FIGURE 8: TIME RESPONSE OF BUTANEDIONE LUMINESCENCE FOR LOW LEVELS OF ILLUMINATION, CASE B.

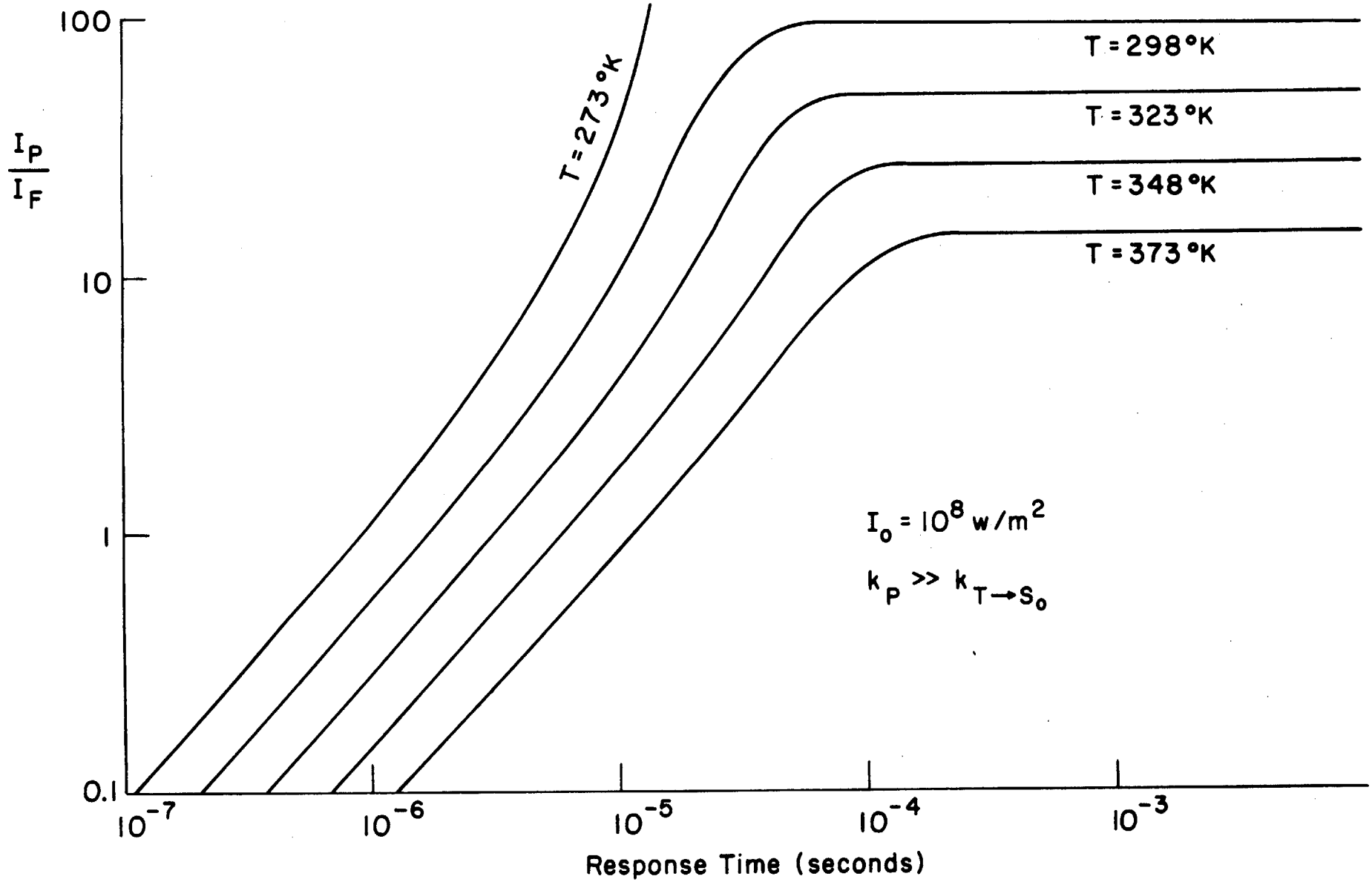

FIGURE 9: TIME RESPONSE OF BUTANEDIONE LUMINESCENCE FOR HIGH LEVELS OF ILLUMINATION, CASE B.